

Gray matter concentration and effective connectivity changes in Alzheimer's disease: a longitudinal structural MRI study

Xingfeng Li · Damien Coyle · Liam Maguire ·
David R Watson · Thomas M McGinnity

Received: 23 July 2010 / Accepted: 27 October 2010 / Published online: 27 November 2010
© Springer-Verlag 2010

Abstract

Introduction Understanding disease progression in Alzheimer's disease (AD) awaits the resolution of three fundamental questions: first, can we identify the location of "seed" regions where neuropathology is first present? Some studies have suggested the medial temporal lobe while others have suggested the hippocampus. Second, are there similar atrophy rates within affected regions in AD? Third, is there evidence of causality relationships between different affected regions in AD progression?

Methods To address these questions, we conducted a longitudinal MRI study to investigate the gray matter (GM) changes in AD progression. Abnormal brain regions were localized by a standard voxel-based morphometry method, and the absolute atrophy rate in these regions was calculated using a robust regression method. Primary foci of atrophy were identified in the hippocampus and middle temporal gyrus (MTG). A model based upon the Granger causality approach was developed to investigate the cause–effect relationship over time between these regions based on GM concentration.

Results Results show that in the earlier stages of AD, primary pathological foci are in the hippocampus and entorhinal cortex. Subsequently, atrophy appears to subsume the MTG.

Conclusion The causality results show that there is in fact little difference between AD and age-matched healthy control in terms of hippocampus atrophy, but there are

larger differences in MTG, suggesting that local pathology in MTG is the predominant progressive abnormality during intermediate stages of AD development.

Keywords Voxel-based morphometry · Longitudinal structural MRI · Effective connectivity · Alzheimer's disease · Hippocampus and medial temporal gyrus

Introduction

Alzheimer's disease (AD) has been extensively studied using cross-sectional structural magnetic resonance imaging (sMRI) methods [1, 2]. Most studies have employed morphometric approaches [3–6] and consistently report gray matter (GM) changes in the hippocampus, entorhinal cortex (EC), and temporal lobe [1, 2, 7, 8]. Although such studies identify regions implicated in the neuropathological processes associated with AD, they can shed no light on individual change over time. To overcome this limitation, several longitudinal sMRI studies have been undertaken [9–18]. Such studies have the advantage of providing more efficient estimators of illness trajectory in terms of neuropathological progression pattern and rates of spread as the illness subsumes new territories of the neocortex. For example, the structural changes in amnesic mild cognitive impaired (aMCI) patients has been longitudinally assessed using whole-brain morphometry [9], where changing atrophy patterns have been identified as subjects progress from aMCI to AD [12]. There is evidence of a particularly rapid atrophy of the hippocampus in aMCI and AD patients in the earlier stages of the disease [16].

X. Li (✉) · D. Coyle · L. Maguire · D. R. Watson ·
T. M. McGinnity
Intelligent Systems Research Centre, Magee Campus,
University of Ulster,
Derry BT487JL Northern Ireland, UK
e-mail: x.li@ulster.ac.uk

Typically, in the study of atrophy progression, regression methods are applied for analysis of the time-dependent data as a function of some predictor variables [19]. Application of transition models such as the Markov general linear model [20] can also be used to trace the pathology characteristic of disease progression [16]. This is a simple procedure which includes past response covariates in the model but does not include interaction terms so it cannot assess any causality feedback interactions (effective connectivity) between affected structures in the longitudinal data. Causality relationships between regions in AD are potentially important. For example, Whitwell [21] has argued that such approaches provide unique insights into region-specific variation and region-specific inter-dependencies of pathology development. To address both feed-forward and feedback causality issues, feedback [19] or Granger causality (GCM) [22] models can be adopted.

The objectives of this study are to combine longitudinal sMRI data with a causality analysis in a large population of prodromal AD and AD patients to address three questions in disease progression. First, *what is the pattern of neuropathological expansion in AD and which regions show earliest disease effects?* Previous studies implicate regions of the hippocampus and EC early in the course of illness, with later pathology extending to include medial temporal lobe (MTL) and middle temporal gyrus (MTG) structures [12, 23]. However, these findings are based on relatively small subject groups, so typicality, in terms of disease progression, is uncertain. In this large-scale study, we test the hypothesis that this progression pattern in AD is indeed characteristic of the disease course. The second question we seek to answer is, *whether the atrophy rates (GM loss) noted in AD is similar or different across affected regions?* This includes analysis of hemisphere-related pathological asymmetry. For example, recent AD studies which estimated the atrophy rate based on brain regional volume [15, 24–26] suggest that hippocampus atrophy may be faster than that seen in MTG; we anticipate that analysis of this large longitudinal population will confirm this finding. Third, *a fundamental question is whether patterns of atrophy across affected regions are inter-dependent or independent, i.e., is there any causality relationship between for example hippocampus atrophy in earlier stages of disease and the MTG atrophy present at later stages of the disease?* Previous work by Nestor and colleagues [10] suggest that the degree and rate of pathology development may be a local phenomenon rather than “inheriting” pathology from other more remote structural entities. We predict that progressive hippocampal changes will be predominantly influenced by a previous state of atrophy in this structure. However, in relation to other temporal regions, we

hypothesize that, although these will again be primarily influenced by their local atrophy characteristics, there will also be an additional influence from the hippocampus condition on this progression.

Materials and methods

Subjects

The data were obtained from the Open Access Structural Imaging Series (OASIS, <http://www.oasis-brains.org/>) database, generously contributed by Dr. Randy Buckner [27, 28]. The data acquisition conformed to The Code of Ethics of the World Medical Association (Declaration of Helsinki), printed in the *British Medical Journal* (18 July 1964). One hundred and fifty subjects (63 males) aged 60 to 96 were included in the study. Each subject was scanned on two or more visits. All scan intervals (from initial scan) were rounded to the nearest year e.g., a scan occurring less than 6 months post-initial scan would be classified as year 0 while a scan occurring 6 months or more later would be classified as year 1 and so on. The analysis was made up of 373 imaging sessions. For each subject at each visit, three or four individual T1-weighted MRI scans are included in the database. The subjects were all right-handed and included both men and women. All subjects were classified according to accepted guidelines using the clinical dementia rating scale (CDR), a key scale in determining dementia of the Alzheimer type [29]. Seventy-two of the recruited subjects were designated as normal aging (age matched healthy controls) throughout the study. Sixty-four others were classified as suffering from some stage of dementia of the AD type at first attendance and remained so classified at subsequent scans, including 51 individuals diagnosed with very mild (CDR=0.5) and 13 mild to moderate (CDR>0.5) dementia of the AD type. Fourteen classified as normal aging at first presentation were subsequently reclassified as suffering some level of dementia consistent with AD on one or more later visits. For the purposes of this longitudinal morphometric comparison, we regarded these 14 converters as AD subjects. The mean age of the AD patients (64+14 subjects; 40 males) was 77.0 (± 7.2), and the mean age of the healthy control subjects (19 males) was 77.1 (± 8.1). The age of the AD patients was not significantly different from that of the controls ($t=0.1014$ nonsignificant at $p<0.05$). The mean mini-mental state examination (MMSE) score was 25.4 (± 4.4) for the AD patients and 29.2 (± 0.9) for control subjects. The MMSE score of the controls was significantly different from that of the AD patients ($t=11.6805$, $p<0.05$). The AD subjects were clinically diagnosed with very mild to moderate AD: CDR=0.5, very mild dementia; CDR=1, mild dementia; CDR=2, moderate

dementia [30]. The CDRs of the 78 subjects in the AD group are between 0.5 and 2 (only two subjects had a CDR of 2).

Structural MRI acquisition

All sMRI were collected with a 1.5-T scanner (Vision, Siemens, Erlangen, Germany). Structural images were acquired with a transmit–receive circularly polarized head coil, and a T1-weighted magnetization prepared rapid gradient-echo sequence (TR [recovery time]=9.7 ms; TE [echo time]=4 ms; flip angle=10°), giving 128 (gap 1.25 mm) sagittal slices of 256×256 image voxels with a voxel size of 1×1×1.25 mm. No neuroimaging evidence of focal lesions such as brain tumors was found, and neither cortical nor subcortical vascular lesions were visible on the structural images.

Structural MRI processing

The pipeline for the sMRI data processing is shown in Fig. 1. For each subject visit, three or four individual T1-weighted MRI scans were averaged to increase the signal-to-noise ratio. These averaged structural images of each of the 373 sessions were registered to the conventional affine Talairach space [31] by the *mritotal* function provided by MINC tools software (<http://noodles.bic.mni.mcgill.ca/ServicesSoftware/HomePage>) to improve the registration in FSL (<http://www.fmrib.ox.ac.uk/fsl/>). If a scan was misregistered (each image was checked visually) by *mritotal*, then the manual control point registration method was performed using *register* software from MINC tools. The averaged structural images were re-sampled to 2×2×2 mm (FSL can only process the data with maximum image resolution of 2×2×2 mm) and transformed to Talairach space for FSL-VBM software analysis (for details: <http://www.fmrib.ox.ac.uk/fsl/vbml/index.html>) by using a *mincresample* function with trilinear interpolation in MINC tools. Then FSL-VBM pre-processing (Fig. 1 solid line blocks) was conducted as follows. First, the BET method [32] was employed to extract the brain (cut the skull from whole image) from the averaged and re-sampled structural image for each of the 373 image sessions. Next, non-uniformity correction was carried out, and FAST4 [33] was used to segment tissues according to their type. The segmented GM partial volume images were then aligned to the Montréal Neurological Institute (MNI) standard space (MNI152) by applying the affine registration tool FLIRT [34] and nonlinear registration FNIRT methods, which use a B-spline representation of the registration warp field [35]. The registered images (before smoothing) were averaged to create a study specific template, and the native GM images were then nonlinearly re-registered to the template image. The registered GM partial volume images were then

modulated (to correct for local expansion or contraction) by dividing them by the Jacobian of the warp field. The segmented and modulated images were then smoothed with an isotropic Gaussian kernel with a full-width-at-half-maximum=12 mm using SPM5 (<http://www.fil.ion.ucl.ac.uk/spm/>) with VBM 5.1 (<http://dbm.neuro.uni-jena.de/vbm/vbm5-for-spm5/>) software packages (SPM 5-VBM 5.1). The result images are projected from the MNI space to the Talairach space.

For the longitudinal VBM comparison, if the subject had two visits (visit 1 was denoted as time point 1 and visit 2 was represented as time point 2), we used all sMRI data from both visits for the comparison. If the subject had three visits, we only used the first visit as time point 1 and last visit as time point 2 for the VBM comparison. If the subject had four or five visits, we used the first two visits to create an average of GM concentration as time point 1, and the last two visits to create an average GM concentration for time point 2 for the VBM comparison. The interval between time points 1 and 2 was always at least 1 year (only one subject (subject OAS2_0048) has two MRI scans within 1 year). The date of the scan information (“oasis_longitudinal.csv” file) of the MRI scan can be downloaded from the OASIS website (<http://www.oasis-brains.org/>). It should be noted that in our VBM analysis, both AD and AD converters have been combined to form the patient population. Two separate VBM analyses were conducted: the first compared GM concentration between normal aging subjects with AD patients at time point 1 and the second VBM repeated the comparison for time point 2. A whole-brain voxel-based two-sample *t* test analysis (equal variance) was performed (SPM 5-VBM 5.1). All the default parameters for the *t* test were accepted except the absolute threshold for the GM which was set to 0.01. The significance threshold with the family-wise error (FWE) [36] corrected threshold was set to be $p < 0.05$.

To help localize GM differences, the 116 regions specified in the automated anatomical labeling (AAL) template [37] were used to label regions in the resulting statistical maps. Finally, the atrophy rate within each of the identified regions of GM loss was estimated using a robust linear regression method [38] at the group level (second-level analysis) [39].

To study the effective connectivity between the hippocampus and MTG, a network as shown in Fig. 2 was constructed. Then, a GCM (Appendix 1) with feedback was developed for each subject. For the causality analysis, only the subjects who had at least three visits were used in the analysis, including 20 AD subjects and 34 healthy controls. The GCM needs at least three visits to solve the equation (Eq. A2 in Appendix) for each individual subject. After deriving the model and its parameters, Granger causality inferences (Appendix 2) were employed, and an *F* test was applied to test the causality inference for each subject

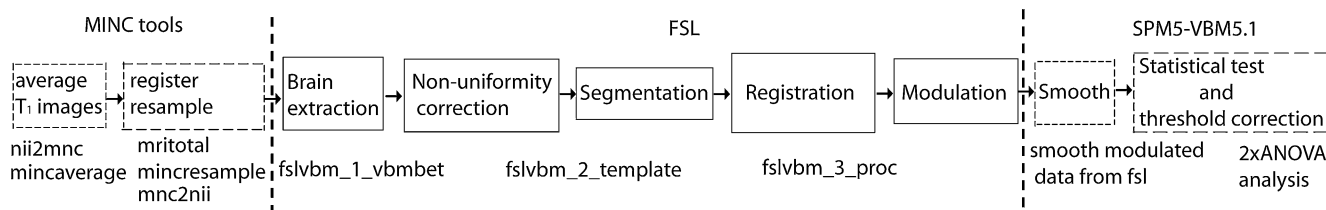


Fig. 1 sMRI data pre-processing steps and VBM analysis. The different software tools used at various stages are indicated above the block diagrams, and functions employed from the software are given

(see Appendix 3). For the second-level analysis [40], a mixed effect model was used to compare causality in the control subjects and AD patients (see Appendix 4).

Results

Localization of cortical atrophy with longitudinal VBM (to address question 1)

The results of the VBM analysis investigating regions of GM concentration change in the AD patients compared to normal aging participants is shown in Fig. 3 at time points 1 (Fig. 3a) and 2 (Fig. 3b). White outlines on the cortex image show the anatomical region boundaries (the edges) of the AAL template detected by the *canny* method from the MATLAB function *edge*.

The color regions on the cortex indicate regions where GM concentration was significantly reduced in AD patients. The initial GM deficits are generally bilateral, located in anterior regions of the hippocampus and entorhinal cortex (EC). Smaller regions of the MTG and temporal pole also show deficits. The figure is consistent with a regional expansion of affected areas with time, which fits with the way AD pathology is known to progressively subsume medial temporal structures. By time point 2, there is an observable progression of atrophy in the medial temporal regions. Hippocampus GM loss has also extended so that most of the structure is affected. Increased deficits were also found in the parahippocampus, MTG, and temporal pole with evidence of extension into the fusiform and parahippocampal gyri. It is also of interest to note that at time point 1, atrophy changes appear more prominent in the right hemisphere, while by time point 2, changes appear

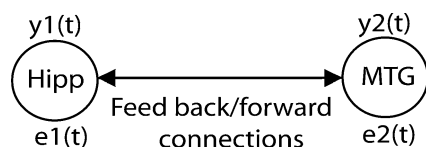


Fig. 2 Hippocampus and MTG network for the effective connectivity study; $y_1(t)$ is the GM concentration from the hippocampus region, and $y_2(t)$ is the GM concentration from the MTG region. $e_1(t)$ and $e_2(t)$ are the model error terms

under the block diagrams. The meaning of each function can be found at the toolbox website, for example, *mritotal* means transfer MRI image to Talairach space

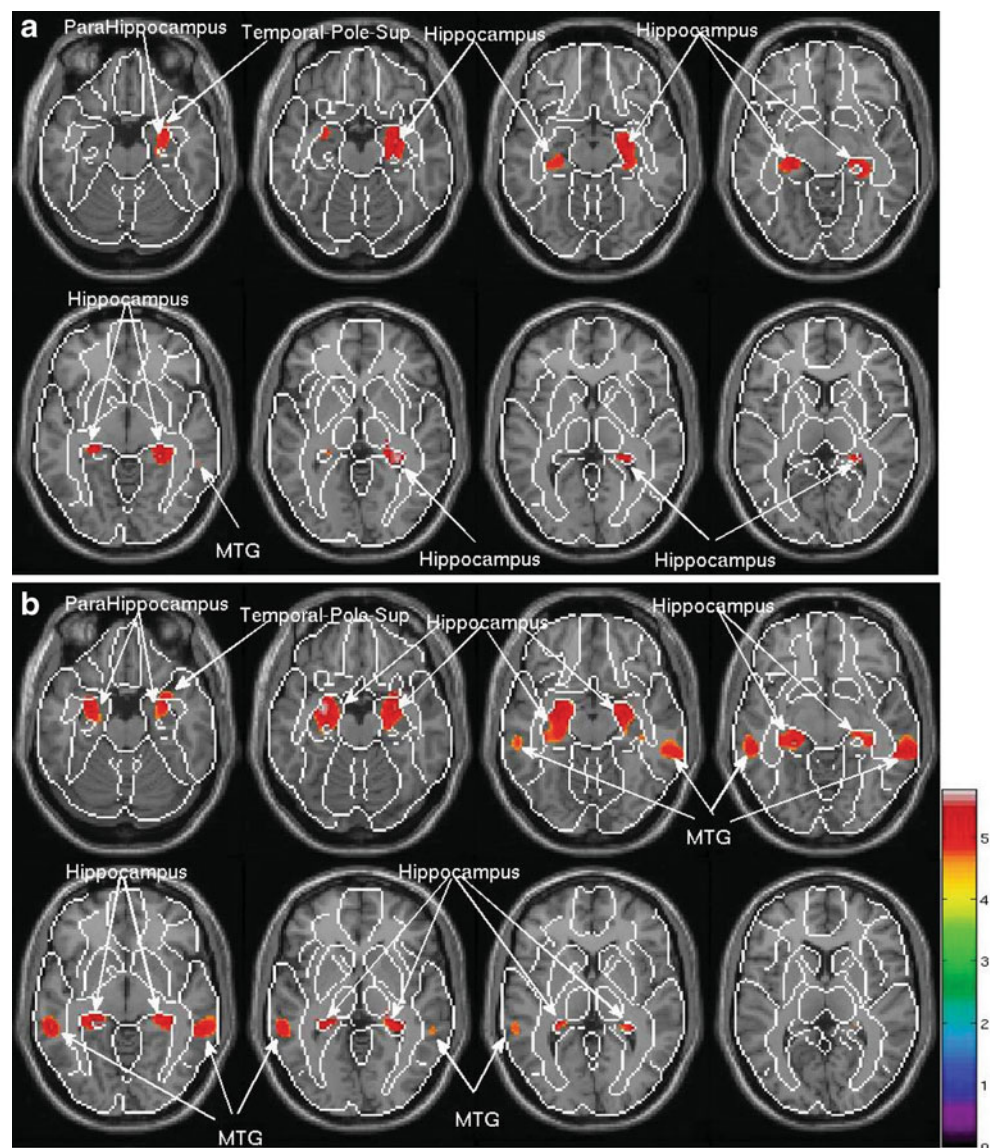
to have progressed more rapidly in the left. In addition, the full factorial model (2×2 ANOVA) was adopted in the VBM analysis which combines the “four groups” (two groups, two time points). We did not find significant difference between time points 1 and 2 in the AD and control group comparison. We further investigated this using a two sample *t* test VBM by setting the contrast matrix to $[1 \ 0 \ -1 \ 0]$ and $[0 \ 1 \ 0 \ -1]$ in full factorial model (the results were exactly the same and not reproduced here). These results confirmed a GM difference between the AD patients and their normal aging counterparts at both time points, predominantly located in the hippocampus and MTG areas. However, the group by time point interaction contrast failed to uncover any significant voxels. This is unexpected and counter intuitively suggests that over the test period, GM changes in both groups were somewhat parallel. However, the analysis method uncouples intra-subject relationships in GM concentration over time, and it is possible that this permits inter-subject variability, which is increased at time point 2 to mask a group influence on differences in rate of atrophy progression.

Atrophy rate estimation in the affected regions (to address question 2)

To further study the atrophy changes in regions showing significant reduction in GM concentration, we employed regional masks to isolate the primary affected regions (hippocampus, MTG) and averaged the GM concentration within these regions for each subject. The first scan was used as the baseline, and subsequent GM changes were estimated by calculating the proportional change (subtracting the first baseline image). Robust linear regression methods [38] were applied to calculate the atrophy rate. The variation in GM concentration over time for the healthy aging and patient groups (patients with dementia at first scan and converters are shown separately) in the hippocampus and MTG are shown in Fig. 4.

The data show that there is a considerable amount of variation across the AD subjects in terms of yearly rate of GM atrophy for both hippocampus and MTG structures, but it is typically 1% for hippocampus and 0.5% for MTG. These rates are, respectively, two times and five times

Fig. 3 VBM analysis results. **a** The comparison results between age matched healthy controls and AD patients at time point 1. **b** The comparison results between age-matched healthy control and AD patients at time point 2. The max and min t values in the color region is $t=4.76$ (min) and $t=5.67$ (max) for **(a)**. The magnitude of the abnormal region in **b** is $t=4.72$ (min) and $t=5.78$ (max). Thresholds corrected for multiple comparisons



greater than rates of atrophy measured in the normal aging controls, both differences are statistically significant when compared to their normal aging counterparts ($p < 0.05$; Fig. 4c). It is also important to note that in the comparison of the atrophy rates between the AD converters (we used seven converted subjects who have at least three longitudinal scans in Fig. 4) and matched controls, no significant difference was noted between the hippocampal atrophy rate; however, the atrophy rate was significantly higher in the MTG for the converter group ($p < 0.05$) suggesting over the period of conversion GM changes in this region are particularly prominent. This is confirmed by the fact that atrophy rates between hippocampus and MTG also significantly differ from one another in this group ($p < 0.05$).

Table 1 and Fig. 5 contain results for the asymmetry analysis. Although Fig. 5 suggests a change in the relative

GM volume (right relative to left hemisphere) in the hippocampus of AD patients compared to controls, this was not confirmed statistically. A two-sample t test showed no significant difference between the asymmetry measures (for either the hippocampus or MTG) between the AD patients and healthy controls, suggesting that the relative (right/left) GM volume in the structures were not altered by disease (Table 1). A hemisphere related asymmetry in GM concentration (Left > Right) was observed for both the hippocampus and MTG which is more marked in the MTG in both populations (Table 1 and Fig. 5). Though it appears atrophy rates are different in the two structures and different in AD and normal aging, this divergence is not profound enough in the present dataset to show statistical difference between groups. This may be because AD subjects are generally in the mild to moderate stage of disease.

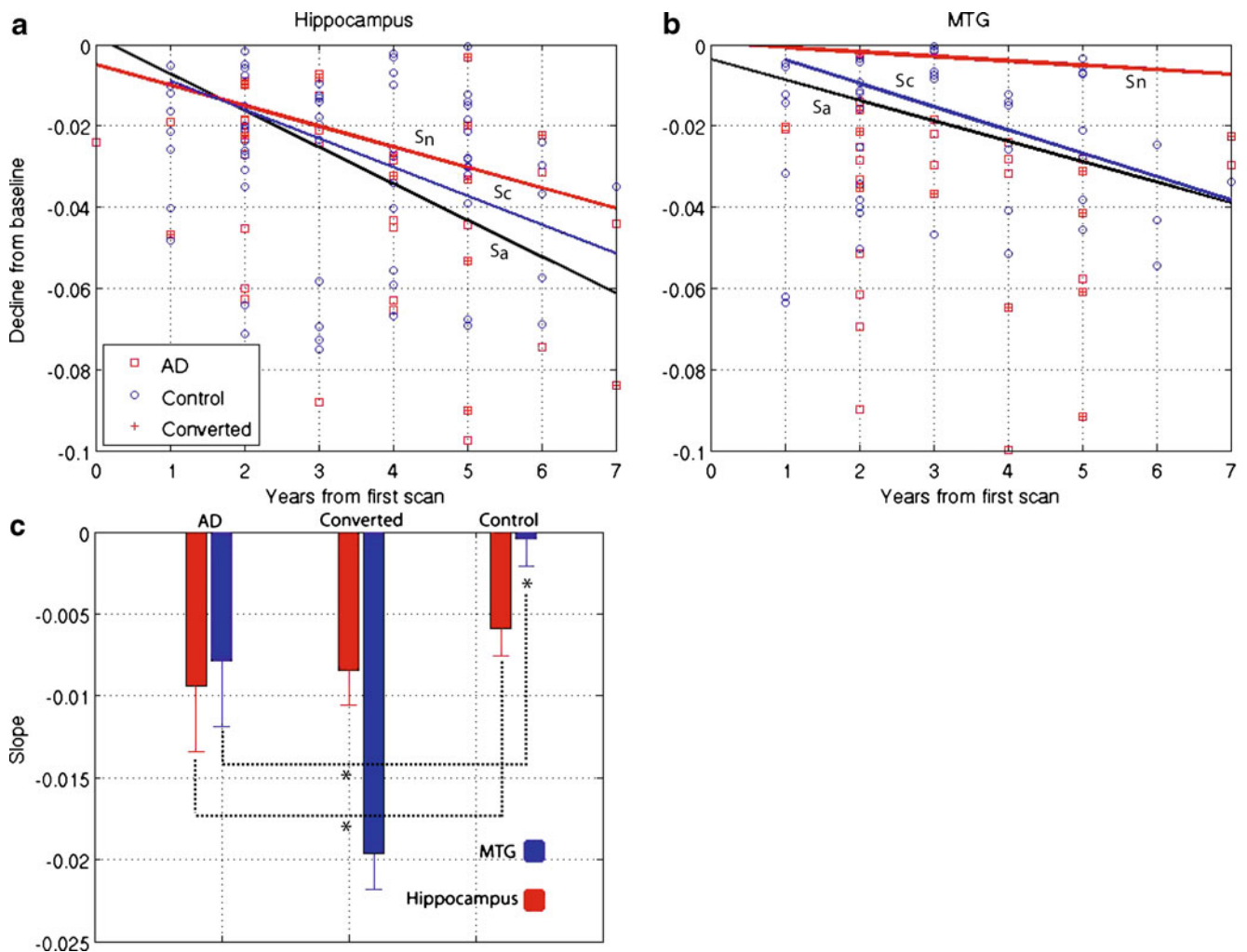


Fig. 4 *Left panel top (a)*, hippocampus GM atrophy annual rate in AD ($S_a = -0.009$), converters ($S_c = -0.007$), and healthy aging ($S_n = -0.005$); *Right panel (b)*, MTG GM atrophy annual rate in AD ($S_a = -0.005$), converters ($S_c = -0.006$), and healthy aging ($S_n = -0.001$). *Left panel bottom (c)* shows comparison of mean atrophy rates for each group (please note one of our subjects from the dataset (subject OAS2_0048)

has five longitudinal scans. For this subject, scans 1, 2, 3, 4, and 5 are collected at the age of 66, 66, 68, 68, and 69, respectively. Using the first scan as baseline, we get an age difference from the first to second MRI scan of 0 and a decline from baseline of -0.02 ; hence, the point at -0.02 at time 0 in (a)

Effective connectivity abnormality in AD (to address question 3)

To estimate the parameters within the GCM to test for effective connectivity (Eq. A2 in Appendix), we required at least three longitudinal scans, which reduced our analysis population to 20 AD subjects and 34 controls. Because of brain symmetry (Fig. 5 and Table 1) and to increase numerical stability, left and right hemispheres were combined in the solution of the GCM equation (Eq. A3 in Appendix 1). A two-connection network was constructed (Fig. 2), and the parameters for the network were calculated (see Appendixes 1 and 2); an F statistic (Appendix 3) was

used to assess significance of inter-region influence (causality). Subsequently, a two-sample t test was employed for group comparisons. The group averaged model for the AD subjects was:

$$y_1(t) = 0.8705y_1(t-1) + 0.0892y_2(t-1) + e_1(t) \quad (1)$$

$$y_2(t) = 0.6652y_1(t-1) + 0.3268y_2(t-1) + e_2(t) \quad (2)$$

where $y_1(t)$ represents the GM concentration in hippocampus of the AD subjects localized as shown in Fig. 3b; $y_2(t)$ denotes the GM concentration in MTG of the AD subjects.

Table 1 Hemisphere symmetry between subject analysis

Correlation coefficient between subject	Time point 1	Time point 2
AD		
Hippocampus	0.8016	0.8125
MTG	0.5693	0.5597
Control		
Hippocampus	0.8888	0.8346
MTG	0.4309	0.6697

The correlation coefficients between left hemisphere and right hemisphere in both groups at time points 1 and 2 (significant at $p < 0.05$)

$e_1(t)$ and $e_1(t)$ are random noise. Similarly, the averaged model for the age matched healthy control subjects was:

$$y_1(t) = 0.8358y_1(t - 1) + 0.1331y_2(t - 1) + e_1(t) \quad (3)$$

$$y_2(t) = 0.4194y_1(t - 1) + 0.5771y_2(t - 1) + e_2(t) \quad (4)$$

F tests values for all the causality (trimmed mean values) are given in Table 2 and Fig. 6a. Figure 6b shows the corresponding coefficients of the feedback model (Eqs. 1, 2, 3, and 4). A mixed effect model (Appendix 4) was employed for the second-level (between-subjects) analysis [40].

Analysis of variance confirms consistent causality relationships between time points 1 and 2 for both structures for both groups ($F(1,52) = 11.152, p < 0.01$). The

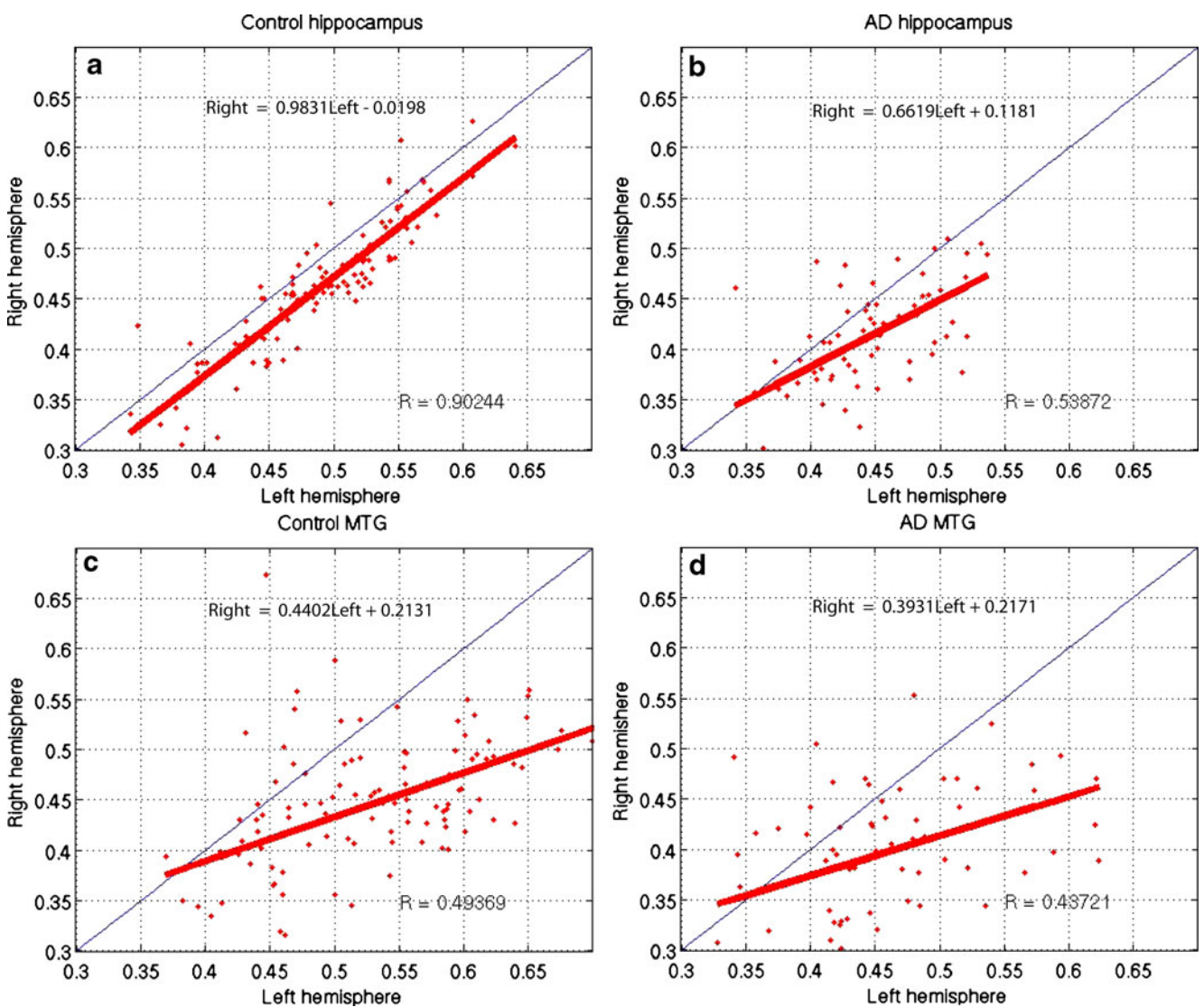


Fig. 5 Scatter plots of relative regional GM concentration in the right and left hemispheres for hippocampus and MTG regions in control and patient groups (averaged across time). **a** Hippocampus of control

subjects; **b** hippocampus of AD subjects; **c** MTG of control subjects; **d** MTG of AD subjects. Regression equations are given within the figure panels

Table 2 Mean F statistics of causality test for GM concentration of hippocampus and MTG for subject groups

Mean F	Hippocampus Local (F1)	MTG to Hippocampus (F2)	Hippocampus to MTG (F3)	MTG Local (F4)
AD	2,375 ($\pm 6,784$)	57 ($\pm 2,540$)	384 ($\pm 3,640$)	419 ($\pm 7,118$)
Normal aging	2,392 (± 896)	95 ($\pm 1,003$)	191 ($\pm 2,260$)	741 (± 746)

All F are significant at $p < 0.05$. The numbers in the table represent mean (\pm standard deviation)

F_1 hippocampus influence from its local past, F_2 influence of hippocampus on MTG, F_3 influence from MTG to hippocampus, F_4 MTG influences from its local past

analysis failed to indicate any group interaction suggesting that this relationship is similar in both the AD and control subjects. The analysis also confirmed a weaker but still significant relationship between regions ($F(1,52) = 4.365$, $p < 0.05$). This suggests that later structural GM concentrations are better predicted by previous concentrations within the same structure and not by a feedback or feed-forward mechanism between structures. There was no evidence of a group interaction suggesting that this inter-structural relationship was not affected by AD (Fig. 6). The difference in causality indices between intra-structural and inter-structural causality was also confirmed in the analysis ($F(1,52) = 20.357$, $p < 0.001$), confirming stronger causality relationships within structures rather than between structures. Several post hoc analyses were also performed. First, we tested to see if there was any evidence of the intra-structural causality found for the hippocampus and the MTG being of differing magnitude (independent of group). The results showed that the causality was greater within the hippocampus than in the MTG ($t(53) = 4.083$, $p < 0.001$). A second analysis to compare directionality effects in inter-structural causality (hippocampus to MTG compared to

MTG to hippocampus) confirmed a greater influence of the hippocampus on the MTG than the reverse situation ($t(53) = -4.286$, $p < 0.001$). To follow this up, we tested to see if the group had any effect on these general relationships. Similar t tests applied on a group basis produced identical results. Suggesting that the causality differences noted above applied equally to both AD and control subjects.

The causality analyses not only confirm relationships between previous and current atrophy states within the hippocampus and MTG but also evidence of temporal relationships between atrophy states across these structures. It is clear from the results that for both the hippocampus and MTG, local changes in GM concentration are the best predictors of future changes. It is also clear that hippocampus atrophy is a better predictor of MTG changes over time than the reverse. Group comparisons of causality indices showed no statistically significant differences. This suggests that the general atrophy patterns encountered in AD are superimposed upon the same causal relationships or linkages upon which normal aging atrophy changes are founded and do not perturb these relationships per se. However, the large increases in statistical variation in the causality data (Fig. 7 and Table 3) for the patient group

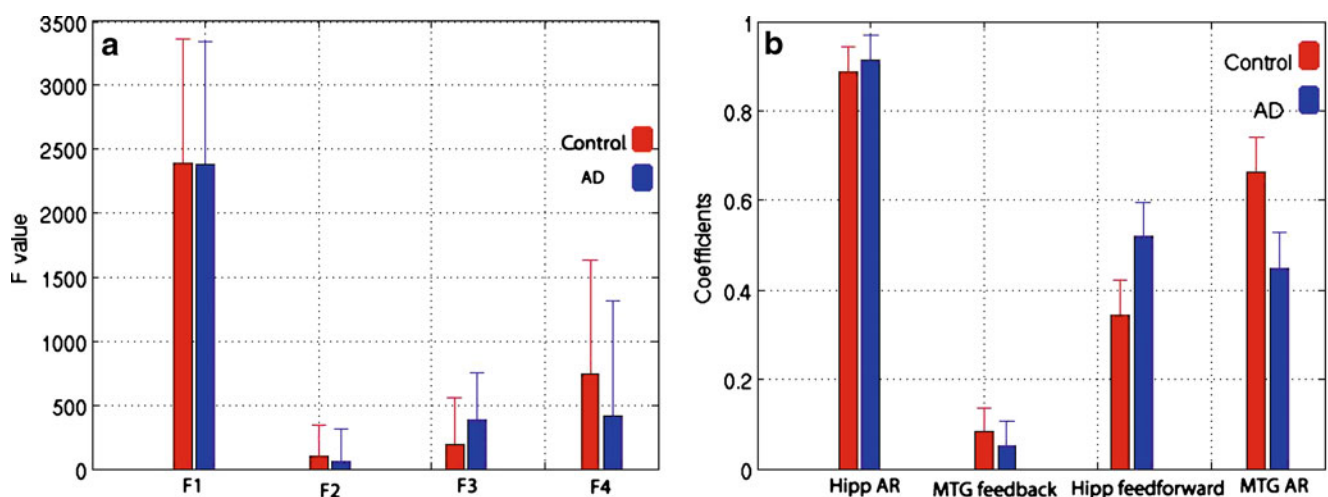


Fig. 6 Group causality analysis comparison results. **a** F test results (left panel). **b** coefficients (right panel) in the feedback model (Eqs. 1, 2, 3, and 4). The figure shows the autoregressive influences within the

hippocampus (F_1 Hippocampus AR) and MTG (F_4 MTG AR); and the mutual/feedback influence between the hippocampus and MTG (F_2 MTG to Hippocampus and F_3 Hippocampus to MTG)

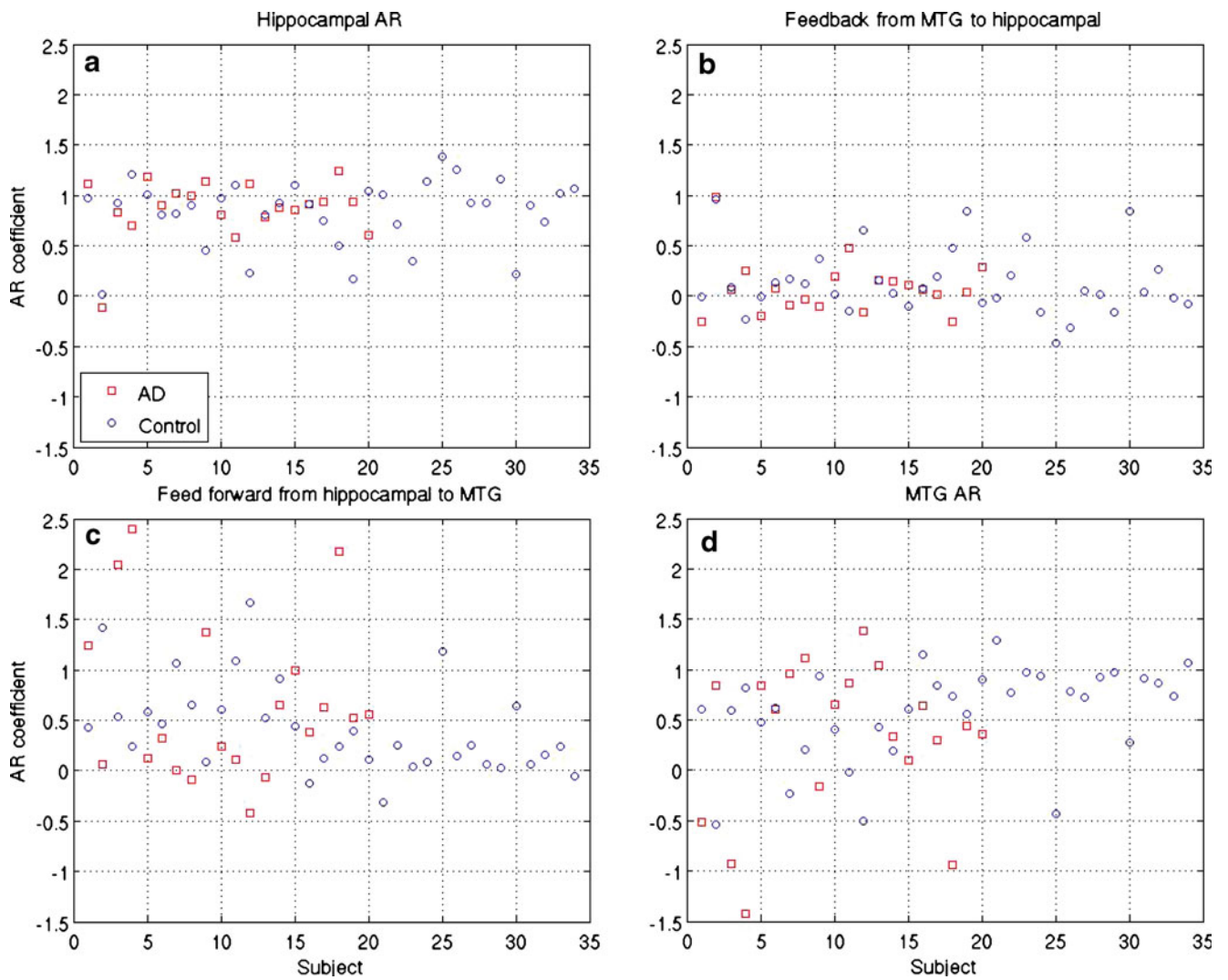


Fig. 7 Feedback model coefficients distribution of normal controls and AD patients. **a** hippocampus autoregression (AR) coefficient; **b** feedback coefficient from MTG; **c** feed-forward influence from hippocampus to MTG; **d** MTG AR coefficients

does suggest that causality relationships are less consistent and may be breaking down in AD subjects compared to their healthy aging counterparts. However, there is no evidence of a uniform trajectory for this breakdown. This may also explain the lack of an observable statistical difference in the group by time point interaction contrast in the VBM analysis.

The coefficient distribution across subjects in the feedback models (Eqs. 1, 2, 3, and 4) are shown in Fig. 7 and Table 3. From Figs. 6b, 7, and Table 3 (mean and

standard deviation of the coefficients), it can be seen that coefficients in the MTG feedback model have a much greater scatter (larger standard derivation) than the hippocampus feed-forward model in both control and AD patients. The lower variability of the causal coefficients within each structure compared to between each structure across the subjects is clearly illustrated in this figure (Fig. 6b). The results of the preceding sections can be summarized as set out in Table 4 below.

Table 3 Coefficients in the feedback model

Model coefficients	Hippocampus auto-regression	MTG feedback	Hippocampus feed-forward	MTG auto-regression
AD	0.871 (± 0.293)	0.089 (± 0.283)	0.665 (± 0.803)	0.327 (± 0.760)
Control	0.836 (± 0.331)	0.133 (± 0.330)	0.419 (± 0.452)	0.577 (± 0.467)

Hippocampus and MTG system feedback model coefficients. *T* test is used for the differences between control and AD subjects. The numbers in the table represent mean (\pm standard deviation)

Table 4 Results summary table

Question	Analysis method	Purpose of investigation	Results	Conclusions
1	VBM Contrast	To quantify the extent of changes in GM concentration in AD.	<p>GM concentration deficits were noted in the hippocampus, EC and MTG in AD patients.</p> <p>GM concentration reduction was present earlier in the hippocampus than other regions of the MTL.</p> <p>Over time hippocampus GM concentration deficits expanded and other regions particularly the MTG begin to show changes.</p> <p>GM concentration deficits showed equal rates of spread in both hemispheres in both AD patients and normal aging controls.</p> <p>GM deficits were more rapid in the hippocampus than in the MTG.</p> <p>Rate of GM deficits were more rapid in the AD patients compared to healthy aged.</p> <p>GM atrophy development is best predicted by current local conditions.</p>	<p>Hippocampus shows GM changes early in illness course.</p> <p>Neuropathology gradually subsumes other areas of the MTL particularly the MTG as illness progresses.</p>
2	Region of interest	Test for hemisphere differences.	<p>GM concentration deficits showed equal rates of spread in both hemispheres in both AD patients and normal aging controls.</p> <p>GM deficits were more rapid in the hippocampus than in the MTG.</p>	<p>Disease processes appear to affect both hemispheres equally.</p> <p>The hippocampus experiences the most rapid atrophy.</p>
3	Causality	<p>Hippocampus and MTG causality.</p> <p>Inter-structural relationships were confirmed but are less important.</p> <p>Intra-structural and inter-structural influences over time.</p>	<p>Rate of GM deficits were more rapid in the AD patients compared to healthy aged.</p> <p>GM atrophy development is best predicted by current local conditions.</p> <p>Inter-structural relationships were confirmed but are less important.</p> <p>Above true for both AD patients and healthy aged.</p> <p>Status of the hippocampus more relevant to atrophy changes in MTG than the reverse in both populations.</p> <p>Evidence of breakdown in inter-structural relationships in AD.</p>	<p>The AD patients showed similar but accelerated patterns of atrophy compared to normally aging subjects.</p> <p>Prior atrophy state is a better predictor of later atrophy state within structures than between structures in both AD and normal aging individuals.</p> <p>Inter-structural relationships are weaker but hippocampus exerts a greater influence on later atrophy in surrounding structures like MTG than vice versa.</p>

Discussion

In this large study, longitudinal VBM methods [5, 9, 41, 42] were employed to map the progression of GM changes in AD. This was done by comparing sMRI images collected at initial referral with images acquired on a second later occasion (one or more years later). The majority of the population studied were considered to be at an early stage in illness progression at first scan as 51 of 64 (80%) had a CDR=0.5 consistent with a very mild stage of the disease of AD type. In addition, a further 14 appeared to be prodromal at this stage. Therefore, in general, time point 1 in the analysis can be considered to represent neuropathology near clinical onset of AD.

Two key regions of atrophy were located bilaterally in the hippocampus and MTG. Absolute qualification of the atrophy rate in these regions was employed to assess whether there were rate differences in GM concentration in these areas. Finally, we carried out a causality analysis to determine patterns of association between the time courses of atrophy accumulation in the hippocampus and MTG regions. Results indicate that in AD, GM loss is extensive; involving large regions of the hippocampus, parahippocampus, MTG, and EC, and so it is not simply loss of effective connectivity in terms of known structural connections which has been reported in some diffusion tensor image studies [43–46]. Further, progression of the disease is fairly rapid and encompasses progressive changes in multiple regions.

Correspondence with previous longitudinal studies

Our results concur with the findings of pathological staging schemes in AD [12, 23, 24], namely that primary neuropathology is first identified in AD in the EC and hippocampus regions (transentorhinal stages I and II), before subsuming temporal lobe structures such as the MTG (limbic stages III and IV). Secondly, the hippocampus showed progressive atrophy throughout the disease course. This is in agreement with other studies [12, 16, 17]. Our results also show that the atrophy rates in the hippocampus were faster than in the MTG in both AD and normal aging subjects, but with a faster rate of change in the AD patients (Fig. 4a). This supports the observation that atrophy rates accelerate as individuals progress further into the disease [24]. It is worthwhile to mention that the unit of atrophy rate in the study is absolute (in proportion). The advantage of using such an absolute unit is that it is straightforward to observe the group decline rate and compare the individual rates across subjects at the same time (Fig. 4). The limitation of this method is that it is unable to quantify the hippocampus volume size change with time. It is interesting to note that the study failed to

find any involvement of the posterior cingulate at both time points. This region has previously been implicated in AD pathology [9, 47]. This is in line with some previous work [12] where posterior cingulate cortex abnormality in AD was not detected. The reason for the discrepancy may be because most of our subjects were in the earlier stages of AD (CDR=0.5); cingulate involvement may, therefore, not have been sufficient to be properly identified. The use of the conservative FWE correction method [36] to correct for multiple comparisons in the VBM analysis may also have contributed in this respect.

Effective connectivity in this study

Although functional [48–54] and structural [49] connectivity abnormalities have been reported in AD, the causality issue [10, 21, 55] of regional atrophy in AD based on longitudinal structural MRI has received little attention. By this, we mean that the temporal pattern of atrophy development, for example, in structures such as the hippocampus, which display earlier evidence of pathology, predict or modulate the way pathology appears and develops in other affected regions as the disease takes hold. Unlike most previous functional connectivity studies which used functional MRI with task-free (resting-state) conditions [49, 53, 54]; we used the GM concentration extracted from the sMRIs to study the effective connectivity. The advantage of this approach is that it has better spatial resolution and, thus, provides increased confidence in localization of the affected brain regions in AD. Furthermore, the functional connectivity approach [56] relies on the correlation; therefore, it is limited in that it cannot address the question of causality between different brain regions. We employed a causality model similar to the work of Granger [22] which is a feedback model [19] and was based on the proposal that there were causality relationships between hippocampus and MTG GM losses over time. This method relied on local current GM values in these regions having a causality relationship with their own past. This model, also named the Markov chain model [20], has been applied to study AD progression previously [16]. We found there were significant influences of atrophy changes over time in the hippocampus on temporal patterns of MTG GM change and vice versa in both AD and their normal age-matched controls. We found there was stronger feed-forward from the hippocampus to MTG than feedback from the MTG to hippocampus (Table 1). This suggests that the changes in and around the hippocampus act as an influence for the way AD engulfs other regions of the temporal lobe. Having said this, the finding that the autoregressive analysis provided by far the best causality linkages shows that in fact the best overall predictors of future change in both the hippocampus and MTG GM was

in fact their previous atrophy condition. This result supports the findings of previous studies [10] suggesting that local pathology is an important variable for the progression of the disease. It must be noted that there is evidence that MTG local pathology is a weaker predictor of its future condition than the hippocampus. This might implicate stronger network influences from connected regions such as the hippocampus.

Advantages and limitations of the method

The strength of the study is, first and foremost, the involvement of a relatively large number of subjects and scans. We used all the 373 cross-sectional MRI scans from OASIS. Furthermore, our method is primarily a longitudinal one, which overcomes the limitation of cross-sectional designs. In addition, in the sMRI data pre-processing stage, we combined three widely used software packages (MINC tools, FSL, and SPM) for VBM data analysis. One major difference between FSL-VBM 1.1 and SPM 5-VBM 5.1 is that FSL-VBM 1.1 uses a permutation test for the statistical comparison in the last step of VBM analysis, while SPM 5-VBM 5.1 uses a two-sample *t* test. The permutation results often include a lot of abnormal regions in AD compared with the two-sample *t* test method [8]. To get conservative values, we chose SPM 5-VBM 5.1 and adopted a two-sample *t* test for the final group comparison. This enables us to use the strengths of both software packages in the analysis. Lastly, in the regression analysis (Figs. 4a, b, and 5), a robust linear regression method was adopted to overcome the limitation of outlier influence on the atrophy rates estimations.

Several limitations in this study should be noted. Firstly, the time interval between the first and second time points is not the same for all the subjects. This will have the effect of increasing variability of atrophy rate across subjects as smaller intervals will tend to show lower rates and longer intervals higher rates in a two-level (time points 1, 2) analysis. Also, there was considerable variation in subject age at initial recruitment. The analysis makes the assumption that atrophy rate will not be affected by this. This allows us to combine the patients with AD at study onset with those who converted in the study period. However, there is some evidence in this study, from comparisons between AD and AD converter subjects, that rate changes for example in the MTG may be more rapid in earlier stages than later on. Combining these two sets of data for the VBM analysis may have had some effects on results. Although a previous study [57] suggested atrophy rate was linear during the aging processing in healthy subjects, another study [24] showed evidence that atrophy rates may fluctuate in different stages of AD.

Another point to mention is that, unavoidably, patients recruited were not all at the same stage of disease. Although the majority of patients were classified as very mild dementia of AD type there remains the problem as to whether atrophy rate in AD holds a linear or nonlinear course as patients become more impaired.

We employed causality based on the feedback model for the longitudinal dataset. Although there has been no universally accepted definition of causality, it is commonly accepted that the notion of causality of two events describes to what extent one event is caused by the other [58]. In the analysis, most of the subjects have three time points (three visits); more longitudinal scans would be needed for more accurate estimates of the causality relationships. This is because the coefficients can contain estimation bias [59] for short time series, especially for the auto-correlation models. Although we combined the left and right hemisphere data to reduce the estimation bias, this only partially offsets the lack of time points in the series. Finally, for the causal model used in this study, we only included linear influences, nonlinear influences were neglected. A nonlinear method [60] with more connected regions and time points could be used to study effective connectivity in future studies in attempts to more fully explore causality relationships.

Finally, it should be pointed out that our causality analysis is based on the averaged concentration of GM in regions of hippocampus and MTG which of course assumes regular atrophy rates across each of the structures; this assumption may not be correct. There is some evidence for example that not all regions of the hippocampus are affected equally in AD as the disease develops with suggestions of an anterior to posterior progression [12].

Conclusion

In conclusion, this investigation provides the following answers to the three posited questions from the data used in this analysis: (1) *what is the pattern of neuropathological expansion in AD?* In the early phase of AD, progression appears to encompass the hippocampus and EC regions, with development of increasing pathology in other regions particularly the MTG region over time. (2) *Are there similar atrophy rates within affected regions in AD?* Affected regions appear to have different atrophy rates, and our results suggest faster atrophy rates in the hippocampus over several years near illness onset. (3) *Is there evidence of causality relationships between different affected regions in AD progression?* The data suggest that local pathology is important for AD progression in affected regions, but there is evidence that magnitude of hippocampal changes may be a factor for increasing MTG abnormality in AD. Interest-

ingly, similar patterns of atrophy progression and causality relationships were found in the normal aging subjects. This suggests that the pathological processes underpinning AD amplify brain changes present during the normal aging process.

Acknowledgments This study is supported under the CNRT award by the Northern Ireland Department for Employment and Learning through its "Strengthening the All-Island Research Base" initiative. The authors thank Dr. Randy Buckner and his colleagues for making their OASIS data available to us. They were supported by Grants No.: P50 AG05681, P01 AG03991, R01 AG021910, P50 MH071616, U24 RR021382, and R01 MH56584.

Conflict of Interest We declare that we have no conflict of interest.

Appendix 1: AR model within subjects for effective connectivity study

For the subjects who have at least three longitudinal scans, we assume the brain GM concentration is an autoregressive (AR) function, i.e., the GM change at a later time point is related to the GM at a previous time point. This is a reasonable assumption [16], and based on this assumption, for each affected region i , we have:

$$y_i(t) = a_i y_i(t - 1) + e_i(t) \tag{A1}$$

where t is the time, $y_i(t)$ is current GM concentration value; $y_i(t - 1)$ is the previous GM concentration value; a_i is the AR coefficient; and $e_i(t)$ is the model error (Gaussian noise). For two-connected regions, we can consider the mutual interaction between these regions (for example hippocampus and MTG as shown in Fig. 2); we thus have a GCM as follows [19, 22]:

$$y_2(t) = b_1 y_1(t - 1) + b_2 y_2(t - 1) + e_2(t) \tag{A2}$$

where $y_1(t)$ and $y_2(t)$ are the current averaged GM concentration in hippocampus and MTG, respectively, and $y_1(t - 1)$, $y_2(t - 1)$ are the corresponding previous average GM concentration in hippocampus and MTG regions as shown in Fig. 3b. If a subject has been scanned only twice over time, we cannot estimate the coefficients based on individual subjects. Equation A2 has two parameters, but two "visits" can only produce one equation. Assuming for each subject, left and right hemispheres have the same model within each subject (Fig. 5), we can build a general linear model for each subject and combine the left and right hemisphere regional GM concentration within this model, i.e. first-level analysis for Eq. A2 [39]:

$$Y = X_1 b_1 + X_2 b_2 + e(t) \tag{A3}$$

where $Y = [y_{2,1}(t), y_{2,2}(t), \dots, y_{2,n}(t)]'$, $n = (V - 1) \times 2$, where V is the total number of visits (we multiply by 2

because we combine the left and right hemisphere GM concentrations within the model); $X_1 = [y_{1,1}(t - 1), y_{1,2}(t - 1), \dots, y_{1,n}(t - 1)]'$, $X_2 = [y_{2,1}(t - 1), y_{2,2}(t - 1), \dots, y_{2,n}(t - 1)]'$. X_2 represents the AR term of $y_2(t)$, and X_1 denotes the influence from the other connected region and $e(t) = [e_{2,1}(t), e_{2,2}(t), \dots, e_{2,n}(t)]' \sim N(0, \sigma^2)$. The estimated GM concentration response is:

$$\hat{Y} = X\hat{\beta} + e(t) \tag{A4}$$

where $\hat{\beta}$ can be estimated by:

$$\hat{\beta} = X^+ Y \tag{A5}$$

and $X = [X_1, X_2]$, and X^+ is the Moore–Penrose pseudoinverse of the matrix. To study the influence from MTG to hippocampus, we swap the $y_2(t)$ and $y_1(t)$ in Eq. A2.

Appendix 2: Granger model for the effective connectivity

Granger causality analysis [61, 62] is derived based on F statistics. For Eq. A2, the test for determining Granger causality (GC) is: (1) $y_1(t)$ is GC of $y_2(t)$ [61], if $b_1 = 0$ in Eq. A2 is not true. Given the data, we reach this conclusion if $b_1 = 0$ is rejected. (2) Similarly, $y_2(t)$ is GC of $y_1(t)$ can be investigated by reversing the input–output roles of the two series. F statistics (see Appendix 3) are developed to detect significant relations within subject, and t statistics are developed for between-subjects analysis (Appendix 4).

Appendix 3: F test (within subject)

After the covariates and their coefficients b_1 and b_2 in Eqs. A3/A4 have been estimated by the least squares method in Appendix 1 from the GM concentration response, the F test [63] is applied to test the inference of the connectivity between different regions. Accordingly from Eq. A4, we partitioned the coefficients $\hat{\beta}$ as: $\hat{\beta} = (\hat{\beta}_1 : \hat{\beta}_2)$ and $X = (X_1 : X_2)$, we can write this test as:

$$H_0: \hat{\beta}_2 = 0 \text{ versus } H_1: \hat{\beta}_2 \neq 0;$$

For one GM concentration response, the F test on the causality is given by [64]:

$$\frac{R^2}{1 - R^2} \frac{n - k - s}{s} \sim F(s, n - k - s) \tag{A6}$$

where s is the column of X_2 ; k is the column of X_1 ; n is the total number of visits minus one (multiply by 2 if combining two hemispheres within the brain). $R^2 = \frac{RSS_0 - RSS}{RSS_0}$, where RSS_0 (original system when $\beta_2 = 0$, without interaction terms for the two-connection network (Fig. 2)) and RSS are the

residual sums of squares (when both the AR and feedback terms exists in the system), $RSS_0 = (Y - \hat{Y})' \times (Y - \hat{Y})$ (under H_0); $RSS = (Y - \hat{Y})' \times (Y - \hat{Y})$. Then, we apply Eq. A6 to test the influences between regions.

Appendix 4: Mixed effect model (first level: within subject)

Apart from the F test conducted within subjects, we can also inference an effect by defining a contrast matrix c and using the t statistics, we start from estimation of an effect:

$$E_j = c\hat{\beta} \tag{A7}$$

$j=1, \dots, n$, where n is the number of visits minus one ($\times 2$ if combine two hemispheres within the model in A3/A4). For example, we can select $c=[0,1]$ at first level contrast to study the influence from MTG to hippocampus.

$$S_j = \|cX^+\| \hat{\sigma} \tag{A8}$$

where $\hat{\sigma} = \sqrt{r'r/v}$, $r = Y - X\hat{\beta}$, $v = m - \text{rank}(X)$ is the degree of freedom (df); $m = 2(n - 1)$ is the total number of effect in Eq. A7 for two hemispheres.

Appendix 4: Mixed effect model (second level: between subjects)

For the second-level analysis, a general linear mixed model [65] was adopted, i.e.:

$$E = Z \cdot \gamma + \eta \tag{A9}$$

where $E=(E_1, \dots, E_{n^*})'$, $S=(S_1, \dots, S_n)$, and η is normally distributed with zero mean and variance $S + \sigma_{\text{random}}^2$ independently for $j=1, \dots, n$. We want to compare the effects in VBM using covariates (Z is the design matrix for comparison in the general linear model):

$$Z = \begin{bmatrix} I_{n_1^*} & O_1 \\ O_2 & I_{n_2^*} \end{bmatrix} \tag{A10}$$

If we are interested in the difference between two groups, we can set $I_{n_1} = [1, \dots, 1]_{1 \times n_1^*}$, $I_{n_2} = [1, \dots, 1]_{1 \times n_2^*}$, $O_2 = [0, \dots, 0]_{1 \times n_2^*}$ and $O_1 = [0, \dots, 0]_{1 \times n_1^*}$. In this study, $n_1^* = 34$ (number of controls), $n_2^* = 20$ (number of AD subjects).

To estimate γ in Eq. A9, we first use the restricted maximum likelihood [66, 67] algorithm to estimate $\hat{\sigma}_{\text{random}}^2$. In the expectation maximization algorithm [67–69], let $S = \text{diag}(S_1, \dots, S_{n^*})$ and \mathbf{I} be the $n^* \times n^*$ identity matrix

($n^* = n_1^* + n_2^* = 54$ in this study). From (A9), we have the variance matrix of the effects vector $\mathbf{E}=(E_1, \dots, E_{n^*})'$:

$$\Sigma = \mathbf{S}^2 + \mathbf{I}\sigma_{\text{random}}^2 \tag{A11}$$

Define the weighted residual matrix:

$$R_{\Sigma} = \Sigma^{-1} - \Sigma^{-1} \mathbf{Z} (\mathbf{Z}' \Sigma^{-1} \mathbf{Z})^{-1} \mathbf{Z}' \Sigma^{-1} \tag{A12}$$

Starting with an initial value of $\sigma_{\text{random}}^2 = \mathbf{E}' \mathbf{R}_1 \mathbf{E} / v^*$ based on assuming that the fixed effects variances are zero. The updated estimate is:

$$\hat{\sigma}_{\text{random}}^2 = \left(\sigma_{\text{random}}^2 (p^* + \text{tr}(\mathbf{S}^2 \mathbf{R}_{\Sigma})) + \sigma_{\text{random}}^4 \mathbf{E}' \mathbf{R}_{\Sigma} \mathbf{E} / n^* \right) / n^* \tag{A13}$$

where $p^* = \text{rank}(Z)$. Replace σ_{random}^2 with $\hat{\sigma}_{\text{random}}^2$ in (A11) and iterate (A11–A13) to convergence. In practice, 10 iterations appear to be enough [69]. After convergence, step (A11) is repeated with σ_{random}^2 by $\hat{\sigma}_{\text{random}}^2$, then the estimate of γ is:

$$\hat{\gamma} = (Z' \Sigma^{-1} Z)^+ Z' \Sigma^{-1} E \tag{A14}$$

And its estimated variance matrix is:

$$V\hat{\text{ar}}(\hat{\gamma}) = (Z' \Sigma^{-1} Z)^+ \tag{A15}$$

In the case when the variances of E are not homogeneous across the level 2 unit (for example, different scanner), Eq. A15 should be replaced by other terms [40, 70]:

$$V\hat{\text{ar}}(\hat{\gamma}) = (Z' \Sigma^{-1} Z)^+ Z' \Sigma^{-1} (E - Z\hat{\gamma})(E - Z\hat{\gamma})' \Sigma^{-1} Z (Z' \Sigma^{-1} Z)^+ \tag{A16}$$

Finally, effects defined by a contrasts matrix (second level, $\mathbf{b}=[1 \ -1]$ in this study for control compared to AD) \mathbf{b} in γ can be estimated by $E^* = \mathbf{b} \gamma$ with standard deviation:

$$S^* = \sqrt{\mathbf{b}' V\hat{\text{ar}}(\hat{\gamma}) \mathbf{b}} \tag{A17}$$

The T statistic is:

$$T^* = E^* / S^* \tag{A18}$$

with a nominal ν^* df ($\nu^* = n^* - \text{rank}(Z)$) can then be used to detect such an effect.

References

- Chetelat G, Degranges B, Sayette VDL, Viader F, Eustache, Baron JC (2002) Mapping grey matter loss with voxel-based morphometry in mild cognitive impairment. *NeuroReport* 13:1939–1943
- Karas G, Burton EJ, Rombouts SARB, Schijndel RAV, O'Brien JT, Scheltens PH, McKeith IG, Williams D, Ballard C, Barkhof F (2003) A comprehensive study of grey matter loss in patients with Alzheimer's disease using optimized voxel-based morphometry. *Neuroimage* 18:895–907
- Ashburner J, Friston KJ (2000) Voxel-based morphometry—the methods. *Neuroimage* 11:805–821
- Davies RR, Scahill VL, Graham A, Williams GB, Graham KS, Hodges JR (2008) Development of an MRI rating scale for multiple brain regions: comparison with volumetrics and with voxel-based morphometry. *Neuroradiology* 51:491–503
- Kakeda S, Korogi Y (2010) The efficacy of a voxel-based morphometry on the analysis of imaging in schizophrenia, temporal lobe epilepsy, and Alzheimer's disease/mild cognitive impairment: a review. *Neuroradiology* 52:711–721
- Takao H, Abe O, Ohtomo K (2010) Computational analysis of cerebral cortex. *Neuroradiology* 52:691–698
- Hirata Y, Matsuda H, Nemoto K, Ohnishi T, Hirao K, Yamashita F, Asada T, Iwabuchi S, Samejima H (2005) Voxel-based morphometry to discriminate early Alzheimer's disease from controls. *Neurosci Lett* 382:269–274
- Li X, Messé A, Marrelec G, Pélégrini-Issac M, Benali H (2010) An enhanced voxel-based morphometry method to investigate structural changes: application to Alzheimer's disease. *Neuroradiology* 52:203–213
- Chetelat G, Landeau B, Eustache F, Mezenge F, Viader F, de la Sayette V, Degranges B, Baron JC (2005) Using voxel-based morphometry to map the structural changes associated with rapid conversion in MCI: A longitudinal MRI study. *Neuroimage* 27:934–946
- Nestor PJ, Scheltens P, Hodges JR (2004) Advances in the early detection of Alzheimer's disease. *Nat Rev Neurosci* 7:s34–s41
- Fox NC, Warrington EK, Freeborough PA, Hartikainen P, Kennedy AM, Stevens JM, Rossor MN (1996) Presymptomatic hippocampal atrophy in Alzheimer's disease: a longitudinal MRI study. *Brain* 119:2001–2007
- Whitwell JL, Przybelski SA, Weigand SD, Knopman DS, Boeve BF, Petersen RC, Jack CR Jr (2007) 3D maps from multiple MRI illustrate changing atrophy patterns as subjects progress from mild cognitive impairment to Alzheimer's disease. *Brain* 130:1777–1786
- Chan D, Janssen JC, Whitwell JL, Watt HC, Jenkins R, Frost C, Rossor MN, Fox NC (2003) Change in rates of cerebral atrophy over time in early-onset Alzheimer's disease: longitudinal MRI study. *Lancet* 362:1121–1122
- Schott JM, Fox NC, Frost C, Scahill RI, Janssen JC, Chan D, Jenkins R, Rossor MN (2003) Assessing the onset of structural change in familial Alzheimer's disease. *Ann Neurol* 53:181–188
- Fox NC, Schott JM (2004) Imaging cerebral atrophy: normal ageing to Alzheimer's disease. *Lancet* 363:392–394
- Schuff N, Woerner N, Boreta L, Kornfield T, Shaw LM, Trojanowski JQ, Thompson PM, Jack CR Jr, Weiner MW (2009) MRI of hippocampal volume loss in early Alzheimer's disease in relation to ApoE genotype and biomarkers. *Brain* 132:1067–1077
- Ridha BH, Barnes J, Barlett JW, Godolt A, Pepple T, Rossor MN, Fox NC (2006) Tracking atrophy progression in familial Alzheimer's disease: a serial MRI study. *Lancet Neurol* 5:824–834
- Schill RI, Frost C, Jenkins R, Whitwell JL, Rossor MN, Fox NC (2003) A longitudinal study of brain volume changes in normal aging using serial registered magnetic resonance imaging. *Arch Neurol* 60:989–994
- Zeger SL, Liang KY (1991) Feedback models for discrete and continuous time series. *Stat Sin* 1:51–64
- Diggle PJ, Heagerty P, Liang KY, Zeger S (2003) Analysis of longitudinal data, 2nd edn. Oxford University Press, Oxford
- Whitwell JL (2008) Longitudinal imaging: change and causality. *Curr Opin Neurol* 21:410–416
- Granger C (1969) Investigating causal relations by econometric models and cross-spectral methods. *Econometrica* 37:424–438
- Braak H, Braak E (1996) Evolution of the neuropathology of Alzheimer's disease. *Acta Neurol Scand Suppl* 165:3–12
- Jack CR Jr, Weigand SD, Shiung MM, Przybelski SA, O'Brien PC, Gunter JL, Knopman DS, Boeve BF, Smith GE, Petersen RC (2008) Atrophy rates accelerate in Amnesic mild cognitive impairment. *Neurology* 70:1740–1752
- Jack CR Jr, Shiung MM, Gunter JL, O'Brien PC, Weigand SD, Knopman DS, Boeve BF, Ivnik RJ, Smith GE, Cha RH, Tangalos EG, Petersen RC (2004) Comparison of different MRI atrophy rate measures with clinical disease progression in AD. *Neurology* 62:591–600
- Resnick SM, Pham DL, Kraut MA, Zonderman AB, Davatzikos C (2003) Longitudinal magnetic resonance imaging studies of older adults: a shrinking brain. *J Neurosci* 23:3295–3301
- Marcus DS, Fotenos AF, Csernansky JG, Morris JC, Buckner RL (2009) Open access series of imaging studies: longitudinal MRI data in nondemented and demented older adults. *J Cog Neurosci* 22(12):2677–2678
- Marcus DS, Wang TH, Parker J, Csernansky JG, Morris JC, Buckner RL (2007) Open Access Series of Imaging Studies (OASIS): cross-sectional MRI data in young, middle aged, nondemented, and demented older adults. *J Cog Neurosci* 19:1498–1507
- Morris JC (1997) Clinical dementia rating: A reliable and valid diagnostic and staging measure for dementia of the Alzheimer type. *Int Psychogeriatrics* 9(suppl 1):173–176
- Morris JC (1993) The clinical dementia rating (CDR): Current version and scoring rules. *Neurology* 43:2412b–2414b
- Talairach J, Tournoux P (1998) Coplanar stereotaxic atlas of the human brain. Thieme, Stuttgart
- Smith SM (2002) Fast robust automated brain extraction. *Hum Brain Mapp* 17:143–155
- Zhang Y, Brady M, Smith SM (2001) Segmentation of brain MR images through a hidden Markov random field model and the expectation maximization. *IEEE Trans Med Imag* 21:45–47
- Jenkinson M, Smith SM (2001) A global optimisation method for robust affine registration of brain images. *Med Image Anal* 5:143–156
- Rueckert D, Sonda LI, Hayes C, Hill DLG, Leach MO, Hawkes DJ (1999) Non-rigid registration using free-form deformations: application to breast MR images. *IEEE Trans Med Imag* 18:712–721
- Nichols TE, Hayasaka S (2003) Controlling the familywise error rate in functional neuroimaging: a comparative reviews. *Stat Meth Med Res* 12:419–446
- Tzourio-Mazoyer N, Landeau B, Papathanassiou D, Crivello F, Etard O, Delcroix N, Mazoyer B, Joliot M (2002) Automated anatomical labelling of activations in SPM using a macroscopic anatomical parcellation of the MNI MRI single-subject brain. *Neuroimage* 15:273–289
- Huber PJ (1981) Robust statistics. Wiley, Hoboken
- Bryk AS, Raudenbush SW (1992) Hierarchical linear models: applications and data analysis methods. Sage, New Delhi
- Sullivan LM, Dukes KA, Losina E (1999) Tutorial in biostatistics: An introduction to hierarchical linear modelling. *Statist Med* 18:855–888

41. Draganski B, Gaser C, Busch V, Schuierer G, Bogdahn U, May A (2004) Changes in grey matter induced by training. *Nature* 427:311–312
42. Draganski B, Gaser C, Kempermann G, Kuhn HG, Winkler J, Buchel C, May A (2006) Temporal and spatial dynamics of brain structure changes during extensive learning. *J Neurosci* 26:6314–6317
43. Salat DH, Tuch DS, van der Kouwe AJW, Greve DN, Pappu V, Lee SY, Hevelonea ND, Zalet AK, Growdon JH, Corkin S, Fischl B, Rosasa HD (2010) White matter pathology isolates the hippocampal formation in Alzheimer's disease. *Neurobiol Aging* 31:244–256
44. Zhang Y, Schuff N, Du AT, Rosen HJ, Kramer JH, Gorno-Tempini ML, Miller BL, Weiner MW (2009) White matter damage in frontotemporal dementia and Alzheimer's disease measured by diffusion MRI. *Brain* 132:2579–2592
45. Fellgiebel A, Wille P, Muller MJ, Winterer G, Scheurich A, Vucurevic G, Schmidt LG, Stoeter P (2004) Ultrastructural hippocampal and white matter alterations in mild cognitive impairment: a diffusion tensor imaging study. *Dement Geriatr Cogn Disord* 18:101–108
46. Muller MJ, Greverus D, Dellani PR, Weibrich C, Wille PR, Scheurich A, Stoeter P, Fellgiebel A (2005) Functional implications of hippocampal volume and diffusivity in mild cognitive impairment. *Neuroimage* 28:1033–1042
47. Chetelat G, Villain N, Desgranges B, Eustache F, Baron JC (2009) Posterior cingulate hypometabolism in early Alzheimer's disease: what is the contribution of local atrophy versus disconnection? *Brain* 132:1–2
48. Vincent JL, Snyder AZ, Fox MD, Shannon BJ, Andrews JR, Raichle ME, Buckner RL (2006) Coherent spontaneous activity identifies a hippocampal-parietal memory network. *J Neurophysiol* 96:3517–3531
49. Seeley WM, Crawford RK, Zhou J, Miller BL, Greicius MD (2009) Neurodegenerative diseases target large-scale human brain networks. *Neuron* 62:42–56
50. Haan WD, Pijnenburg YL, Strijers RLM, Made YVD, Flier WMVD, Scheltens P, Stam CJ (2009) Functional neural network analysis in frontotemporal dementia and Alzheimer's disease using EEG and graph theory. *BMC Neurosci* 10:1–12
51. Stam CJ, Haan WDE, Daffertshofer A, Jones BF, Manshanden I, Van Cappellen V, Van Walsum AM, Montez T, Verbunt JPA, de Munck JC, Van Dijk BW, Berendse HW, Scheltens P (2009) Graph theoretical analysis of magnetoencephalographic functional connectivity in Alzheimer's disease. *Brain* 132:213–224
52. Celone K, Calhoun V, Dickerson B, Atri A, Chua EF, Miller SL, DePeau K, Rentz DM, Selkoe DJ, Blacker D, Albert MS, Sperling RA (2006) Alterations in memory networks in mild cognitive impairment and Alzheimer's Disease: an independent component analysis. *J Neurosci* 26:10222–10231
53. Supekar K, Menon V, Rubin D, Musen M, Greicius MD (2008) Network analysis of Intrinsic functional brain connectivity in Alzheimer's Disease. *PLoS Comput Biol* 4:1–11
54. Greicius MD, Srivastava G, Reiss A, Menon V (2004) Default-mode network activity distinguishes Alzheimer's Disease from healthy aging: Evidence from functional MRI. *Proc Natl Acad Sci* 101:4637–4642
55. Lemieux L (2008) Causes, relationships and explanations: the power and limitations of observational longitudinal imaging studies. *Curr Opin Neurol* 21:391–392
56. Bullmore E, Sporns O (2009) Complex brain networks: graph theoretical analysis of structural and functional systems. *Nat Rev Neurosci* 10:186–198
57. Good C, Johnsrude IS, Ashburner J, Henson RN, Friston KJ, Frackowiak RS (2001) A voxel-based morphometric study of ageing in 465 normal adult human brains. *Neuroimage* 14:21–36
58. Faes L, Nollo G, Chon KH (2008) Assessment of Granger causality by nonlinear model identification: application to short-term cardiovascular variability. *Ann Biomed Eng* 36:381–395
59. Shaman P, Stine RA (1998) The bias of autoregressive coefficient estimators. *J Am Stat Assoc* 83:842–848
60. Li X, Marrelec G, Hess RF, Benali H (2010) A nonlinear identification method to study effective connectivity in functional MRI. *Med Image Anal* 14:30–38
61. Wernerheim C (2000) Cointegration and causality in the exports-GDP nexus: the post-war evidence for Canada. *Empirical Econ* 25:111–125
62. Oxley L, Greasley D (1998) Vector autoregression, cointegration and causality: testing for causes of the British industrial revolution. *Appl Econ* 30:1387–1397
63. Doornik J (1996) Testing vector error autocorrelation and heteroscedasticity. *The Econometric Society 7th World Congress*, Tokyo, 1996.
64. Durbin J (1970) Testing for serial correlation in least squares regression when some of the regressors are lagged dependent variables. *Econometrica* 38:410–421
65. Breslow NE, Clayton DG (1993) Approximate inference in generalized linear mixed models. *J Am Stat Assoc* 88:9–25
66. Dempster AP, Laird NM, Rubin DB (1977) Maximum likelihood from incomplete data via the EM algorithm. *J Roy Stat Soc B* 39:1–38
67. Laird NM, Lange N, Stram D (1987) Maximum likelihood computations with repeated measures: Application of the EM algorithm. *J Am Stat Assoc* 82:97–105
68. Laird NM, Ware JH (1982) Random-effects models for longitudinal data. *Biometrics* 38:963–974
69. Worsley K, Liao CH, Aston J, Petre V, Duncan GH, Morales F, Evans AC (2002) A general statistical analysis for fMRI data. *Neuroimage* 15:1–15
70. Liang KY, Zeger SL (1986) Longitudinal data analysis using generalized linear models. *Biometrika* 73:13–22, *Neuroimage* 11:805–821